Inorganic Chemistry

pubs.acs.org/IC Article

Sulfur-Functionalized Single-Walled Carbon Nanotube Buckypaper/MTV-BioMetal−Organic Framework Nanocomposites for Gold Recovery

Mariafrancesca Baratta,[#] Teresa F. Mastropietro,[#] Paula Escamilla, Vincenzo Algieri, Fang Xu, Fiore Pasquale Nicoletta, Jesus Ferrando-Soria, Emilio Pardo,* Giovanni De Filpo,* and Donatella Armentano*

Cite This: *Inorg. Chem.* 2024, 63, 18992−19001 Read Online

ACCESS | Metrics & More | Article Recommendations | Supporting Information

ABSTRACT: Developing sustainable, efficient, and selective gold recovery technology is essential to implement the valorization of complementary alternative sources for this precious metal, such as spent e-waste, and to preserve the environment. The main challenge in recovering gold from liquors obtained from leached waste electronics is the low concentration of this precious metal compared to impurities. Here, we report the preparation of a novel multivariate biological metal−organic framework (MTV-BioMOF) as a potential material for the selective recovery of gold metal ions from water, even in the presence of other interfering metals. Moreover, MTV-BioMOF can be incorporated within single-walled carbon nanotube buckypapers (SWCNT-BP) to yield an MTV-BioMOF@HS-SWCNT-BP composite, which combines enhanced mechanical properties and high chemical stability. The thiol-functionalized SWCNT-BP surface and the presence of thioether groups evenly decorating the MTV-BioMOF channels shape a task-specific functional environment that boosts the interactions with gold metal ions. The efficiency of gold recovery reaches values up to 99.5% when MTV-BioMOF@SWCNT-BP is used as an adsorbent for treating Au(III) in very diluted solutions (initial concentration of 5 ppm). This high recovery efficiency, with values as high as 98.0%, is maintained even in the presence of competing metal cations, also demonstrating a noticeable selectivity. This composite material represents a promising paradigm for the selective extraction, enrichment, and purification of gold.

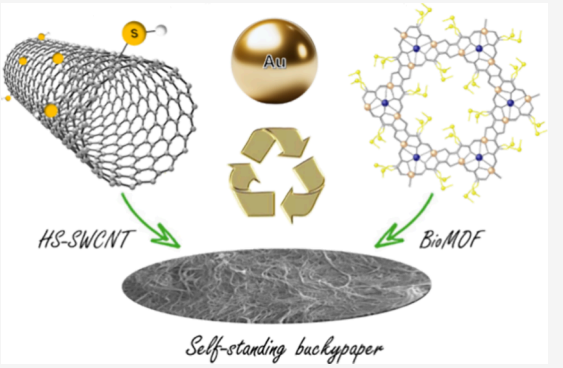

INTRODUCTION

The rapid global development of advanced technology has led to an increased demand of gold metal in recent years and to a growing production of electronic waste (e-waste).[1,2] Since e-waste can contain up to ∼280 g t^{-1} of gold, which considerably exceeds the amount of accessible gold in natural mined ores (3−30 g t^{-1}), it can be reasonably considered as a valuable source of this precious metal.[3,4] Therefore, developing new methods for the efficient and selective extraction and recovery of gold from e-wastes can help to fix the growing demand for gold, contributing at once to the global e-waste management and the reduction of the environmental pollution due to mining practices.[5]

Redox methods are mainly employed to produce leachates containing soluble Au(III) species from solid e-waste. Compared with other leaching agents, the use of aqua regia is relatively inexpensive and simple in operation and reduces the environmental impact derived from the use of more harmful chemicals.[6−8] The main issue arising from the use of these methods is the diversified and complex composition of the leach liquor, which typically contains low ppm levels of gold as other compounds and metal ions, often at a significantly higher concentration.[9−12]

Conventional methods for gold recovery from solution include solvent extraction, chemical precipitation, ion exchange, redox reactions, and adsorption.[13−15] Because of its simple operation, easy scalability, low cost, and high efficiency, adsorption is considered one of the most reliable methods for gold recovery. A variety of adsorbent matrices have been developed for gold capture;[16−18] however, most of them have poor adsorption efficiency and selectivity and lack tunable structures and modifiable functionalities to target their application potential. Accordingly, it is highly desirable to

Received: August 9, 2024
Revised: September 5, 2024
Accepted: September 17, 2024
Published: September 26, 2024

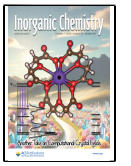

develop adsorbents that have strong affinity for gold to improve their absorption capacity and selectivity.

Metal−organic frameworks (MOFs) have been widely applied as adsorbents because of their structural diversities, feasible modifications, and high and controllable porosity and surface area.[19−22] The introduction of functional groups bearing donor atoms such as O, N, and S can enhance the affinity of MOFs for gold and their adsorption performance.[23] Nevertheless, their use as microcrystalline powder presents some important drawbacks, which make their translation into real-world applications unfavorable.[24,25] Consequently, shaping MOFs into macroscopic robust bodies that can be fitted into the existing industrial processes offers an additional thrust toward their practical use.[26,27]

In this context, some of us have recently reported the preparation of different MOFs based on bioderived ligands, which demonstrated high adsorption capacity and selectivity for the extraction of several metal ions.[28,29] The functional residues derived from the natural amino acids included in the BioMOF structure precisely design a unique coordination environment within the pores, which ensures efficient metal ion recognition and sequestration. To further boost their capture performance, we also focused on the fabrication of BioMOFs with different and controlled functionalities within their channels using different types of organic linkers, the so-called multivariate[30−33] (MTV) MOFs. The modular nature of MTV-MOFs opened up new possibilities in the field of water remediation,[34] making it possible to tailor their porosity with two or more different and cooperative functional groups capable of acting synergistically to capture contaminants of a very different nature at once.[35] These BioMOFs maintained an excellent ability to extract the target metals when embedded in polymeric matrices to prepare mixed matrix membranes as well as when mixed with single-walled carbon nanotubes (SWCNTs) to prepare nanocomposite membrane materials.[36−38] Due to their high surface area, high mechanical resistance, and other remarkable properties, CNTs have recently emerged as an ideal component for the next generation of composite materials for applications in water purification, chemistry of materials, and biomedical sciences.[39] When shaped in the form of buckypapers (BPs), CNTs-BPs combine the characteristics of polymer membranes such as porosity, flexibility, and self-standing ability with those of CNTs, such as thermal stability and mechanical resistance, holding at once the potential in breaking the trade-off between membrane flux and selectivity.[40−43]

With the aim of further investigating the MOF-based technology for precious metal recovery and water remediation, we present in this work a novel, flexible, and robust MTV-BioMOF-based single-walled carbon nanotube buckypaper (**$CaZn_6$MethMecys@HS-SWCNT-BP**) as a potential material for the selective recovery of gold from water, also in the presence of other interfering metals. The MTV-BioMOF@HS-SWCNT-BP composite appears as a very suitable candidate for the selective extraction and purification of gold. Furthermore, the thioether residues decorating the MTV-BioMOF pores and the thiol functional groups on the SWCNT surface are expected to enhance the interactions with gold metal ions.[44] Finally, despite the fact that several examples of thiol-functionalized SWCNTs have been reported, exhibiting remarkable properties, including gold adsorption,[45,46] to the best of our knowledge, their use in BPs has been poorly investigated.[47]

RESULTS AND DISCUSSION

The highly crystalline MTV-BioMOF reported in this work, with the formula $\{Ca^{II}Zn^{II}_6[(S,S)\text{-methox}]_{1.5}[(S,S)\text{-mecysmox}]_{1.5}(OH)_2(H_2O)\}\cdot 12H_2O$ (**$CaZn_6$MethMecys**), was prepared in the gram scale by using oxamidato ligands modified with the natural amino acids L-methionine and *S*-methyl-L-cysteine in a 1:1 molar ratio. It was synthesized according to the synthetic procedure described in the Experimental Section.

Its crystal structure has been determined by single-crystal X-ray diffraction (SCXRD) (Figure 1 and Table S1) and its bulk

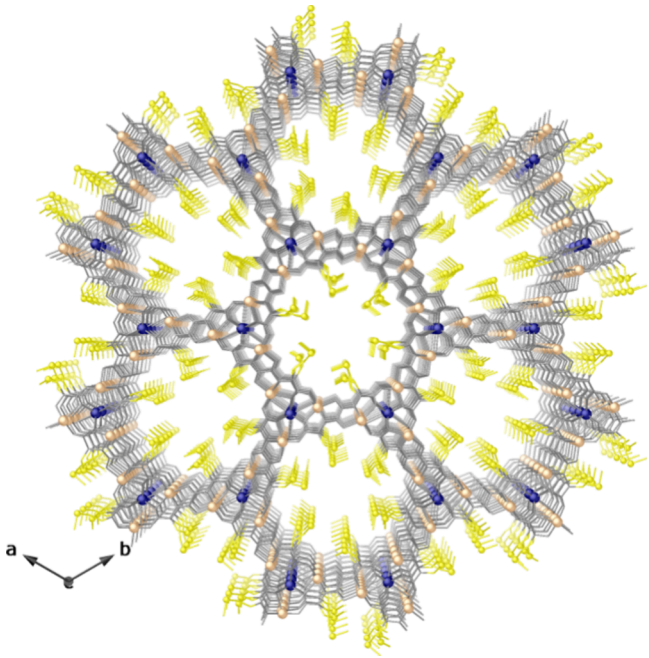

Figure 1. View of the porous crystal structures of **$CaZn_6$MethMecys** highlighting their functional channels decorated with $-CH_2SCH_3$ and $-CH_2CH_2SCH_3$ groups in yellow. Zn and Ca are represented as orange and blue spheres, respectively. Organic ligands are depicted as gray sticks except for sulfur atoms (yellow spheres).

fully characterized through N_2 adsorption isotherms, powder X-ray diffraction (PXRD), and thermogravimetric analysis (TGA) (Figures S1−S3). **$CaZn_6$MethMecys** crystallizes in the $P6_3$ space group, and its structure consists of uninodal **acs** six-connected 3D calcium(II)−zinc(II) networks featuring functional hexagonal channels, where both types of flexible amino acid residues, $-CH_2SCH_3$ and $-CH_2CH_2SCH_3$, of the methylcysteine and methionine, respectively, coexist within the channels (Figure 1 and Figure S4). The six-connected networks are assembled by *trans*-oxamidato-bridged dizinc(II) units of $\{Zn^{II}_2[(S,S)\text{-mecysmox}]\}$ and $\{Zn^{II}_2[(S,S)\text{-methox}]\}$, which are statistically disordered in the crystal structure (Figure S5). The 3D network is built by zinc(II) dimers, which act as metallolinkers between the Ca^{II} ions through the carboxylate groups (Figure S5). Aqua/hydroxo groups (in a 1:2 statistical distribution) further interconnect neighboring Zn^{2+} and Zn^{2+}/Ca^{2+} ions whose result was linked in a μ_3 fashion (Figures S4 and S5). The presence of two types of thioether groups pointing toward the accessible void space of the BioMOFs (Figure 1 and Figure S4), along with the heterogeneity and high flexibility of the porous framework, offers functional channels well-appointed for interacting with

https://doi.org/10.1021/acs.inorgchem.4c03407
Inorg. Chem. 2024, 63, 18992−19001

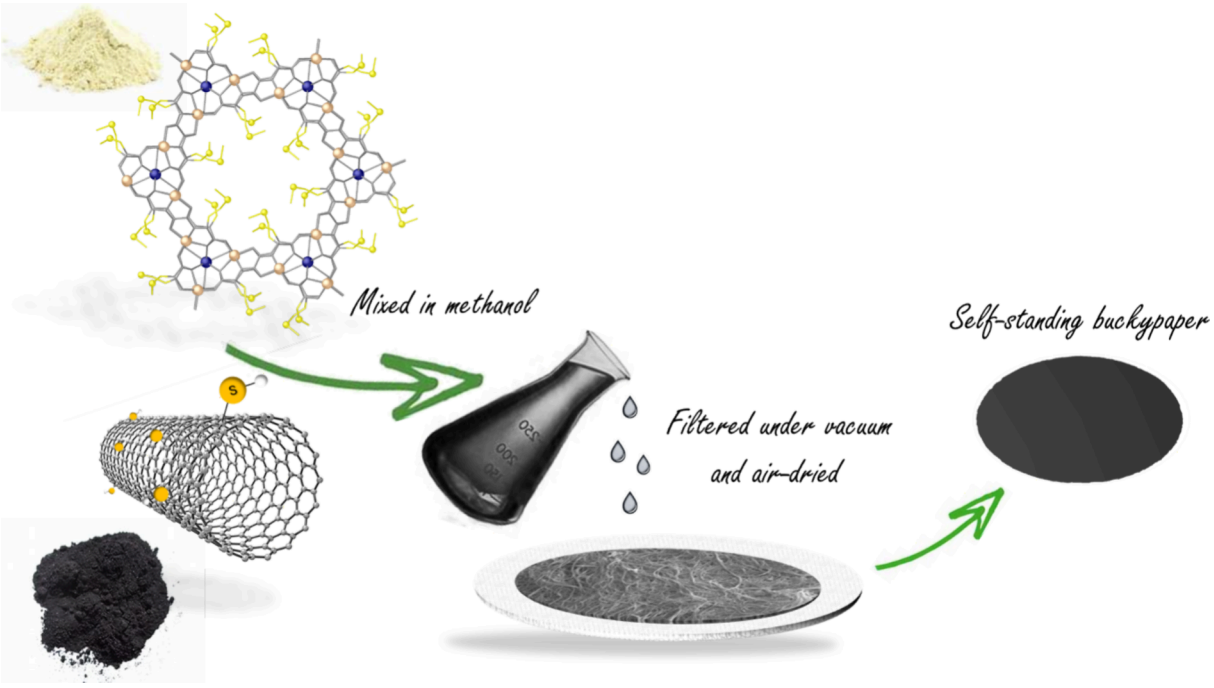

Figure 2. Schematic representation of the procedure applied for the preparation of HS-SWCNT-BP and the **$CaZn_6$MethMecys@HS-SWCNT-BP**.

the softer Au(III) ion, which displays a good binding tendency for sulfur coordination sites.[34,44,48]

The permanent porosity of MTV-BioMOF **$CaZn_6$MethMecys** was confirmed by measuring its N_2 adsorption isotherm (Figure S1). The calculated Brunauer–Emmett–Teller (BET) surface area was 610 m^2/g,[49] with a calculated pore size[50] of 0.65 nm, which is similar to that observed in its crystal structure. The experimental PXRD pattern of polycrystalline samples of **$CaZn_6$MethMecys**, shown in Figure S2, is consistent with the theoretical pattern, thus confirming both the isostructurality of the bulk with the crystals selected for single-crystal X-ray diffraction and the purity of the bulk sample. Finally, the water content shown in the chemical formula of **$CaZn_6$MethMecys** was established by TGA (Figure S3).

The maximum gold uptake capacity of MTV-BioMOF **$CaZn_6$MethMecys** was determined by soaking 5 mg of the polycrystalline powder in 100 mL of a $AuCl_3$ solution with an initial concentration of 20 ppm. ICP-AES analyses indicated a maximum loading of 628 mg/g of Au(III) after 24 h, which is similar to but slightly lower than the value measured for a similar previously reported BioMOF of formula $\{Ca^{II}Cu^{II}{}_6[(S,S)\text{-methox}]_3(OH)_2(H_2O)\}\cdot 16H_2O$.[28]

The SWCNTs employed for the fabrication of the BPs were prior modified with thiol groups following the procedure described in detail in the Experimental Section to produce a task-specific active surface, able to ensure stable interactions with MOF nanocrystals and to improve the adsorption capacities of the BP substrate.[51,52] The procedure implies the preparation of an intermediate sulfurated SWCNT product (SS-SWCNTs). IR spectra of the pristine SWCNTs, the intermediate product SS-SWCNTs, and the final HS-SWCNTs were collected in the region of 4000–375 cm^{-1} to assess the functionalization (Figure S6). In particular, the peak at 571 cm^{-1}, generally assigned to multisulfide bonds and absent in the spectrum of pristine SWCNTs, appears in the spectrum of SS-SWCNT as expected and again disappears in the spectrum of HS-SWCNTs, confirming that the synthesis of HS-SWCNT passes through the formation of S–S bonds before reduction with $NaBH_4$, necessary to convert sulfur bonds into thiolic functions.

To confirm the formation of the thiolic functions on the SWCNTs, XPS spectra were collected (Figure S7). The peak centered at 164.3 eV, which occurs in the XPS spectrum (see the SI) in a region characterized by the S 2p emission of C–S–R (164.5 eV) and C–S–H (163.5 eV) sulfur bonds, validates the success of the thiolation reaction. Moreover, Raman measurements on both samples, SWCNTs and HS-SWCNTs, corroborate the occurrence of HS–C bonds in the latter (Figure S3). The D-band intensity, generally associated with the degree of disorder in the CNT lattice due to the presence of sp^3 bonds, increases by about 31% in the HS-SWCNTs Raman spectrum when compared to that of pristine SWCNTs, thus confirming the presence of HS–C bonds on SWCNTs (Figure S8 and Table S2, SI). By evaluation of these measurements, it is possible to estimate a 7% degree of functionalization in the final HS-SWCNTs product.

The MTV-BioMOF **$CaZn_6$MethMecys**, as a polycrystalline powder, with particle dimensions averaging 0.1 μm, was homogeneously dispersed within a thin (thickness of around 60 μm) BP, made of an entangled network of HS-SWCNTs (Figure S4). The preparation of BP decorated with the MTV-BioMOF nanocrystals is simple and comprises the filtration of a methanolic dispersion of both components in an optimized ratio through a PTFE disk with a vacuum pump followed by drying at room temperature (see the Experimental Section). As reported in the Experimental Section, to preserve the robustness and self-standing properties of the MTV-BioMOF-modified HS-SWCNT-BP, the relative amount of the MTV-BioMOF with respect to the HS-SWCNTs was fixed after several trials to 25%.

Figure 2 shows a schematic representation of the procedure applied for the preparation of the HS-SWCNT-BP and the **$CaZn_6$MethMecys@HS-SWCNT-BP** in the above-mentioned

https://doi.org/10.1021/acs.inorgchem.4c03407
Inorg. Chem. 2024, 63, 18992–19001

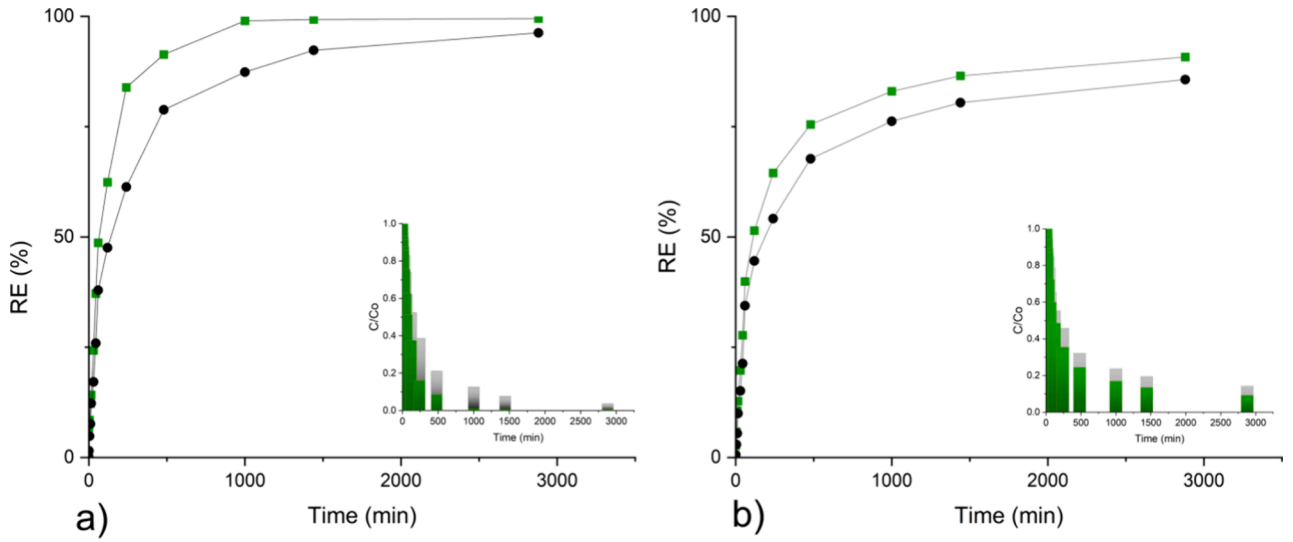

Figure 3. Recovery efficiency (RE%) for gold metal ion by the neat HS-SWCNT-BP (black dots) and the **$CaZn_6$MethMecys@HS-SWCNT-BP** (green dots) during soaking in aqueous solutions of 5 ppm Au^{3+} (volume, 400 mL) at pH 4 (a) and 6 (b) in the 0−48 h interval. Solid lines are guides for eyes. The insets show the variation of the Au^{3+} concentration reported as C/C_0 as a function of time.

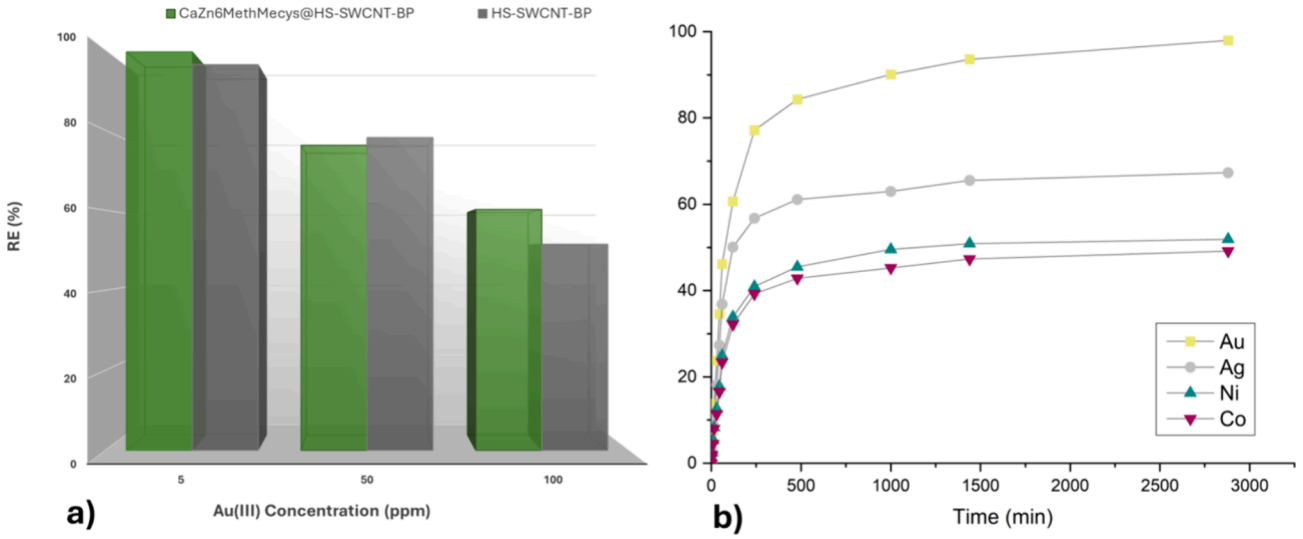

Figure 4. Recovery efficiency (RE%) for gold metal ion by the neat HS-SWCNT-BP and the **$CaZn_6$MethMecys@HS-SWCNT-BP** after soaking in aqueous solutions of 5, 50, and 100 ppm Au^{3+} (volume, 400 mL) at pH 4 (a) and the recovery efficiency (RE%) for gold metal ion in the presence of other interfering metal cations by the **$CaZn_6$MethMecys@HS-SWCNT-BP** during soaking in aqueous solutions of 3 ppm of each metal (volume, 400 mL) at pH 4 (b).

optimized conditions. The circular BPs are characterized by an average thickness of 60 ± 5 μm, an active average diameter of 38 ± 1 mm, and an average mass of 38 ± 2 mg. The morphology of the BPs, assessed by scanning electron microscopy (SEM), is characterized by the presence of a porous and highly disordered structure formed by HS-SWCNTs bundles and clusters of SWCNTs resulting from $\pi-\pi$ and van der Waals interactions (Figure S9a, SI). SEM images collected on the **$CaZn_6$MethMecys@HS-SWCNT-BP** as well as EDX measurements also confirmed the presence and homogeneous distribution of the MTV-BioMOF within the BP (Figures S9b and S10, SI). The MTV-BioMOF forms small spherical aggregates with an average size lower than 1 μm, composed of smaller primary crystallites with an average diameter lower than 0.1 μm. The incorporation of MOFs in the internal structure of the BP membrane leads inevitably to a change in the arrangement that CNTs normally have in BPs due to MOF hosting, which can result in the alteration of mechanical properties of the final composite product. Stress vs strain measurements confirmed that, despite the presence of MOFs, mechanical properties of both topologies of membranes remain quite similar, observing just a slight decrease in the value of stress in **$CaZn_6$MethMecys@HS-SWCNT-BP** membranes (18 MPa in HS-SWCNT-BPs vs 17 MPa in **$CaZn_6$MethMecys@HS-SWCNT-BP**), together with a reduction of about 6% of their elastic properties (Figure S11). Anyway, these values are extremely consistent with measurements on similar BP membranes, both naked and MOF-containing, reported by us in previous work.[38] The highly porous and hydrophilic structure of the HS-SWCNT-BPs stably accommodating the nanosized MTV-BioMOF particles (no leakage was observed during the static adsorption experiments) ensures a large active surface area for the

https://doi.org/10.1021/acs.inorgchem.4c03407
Inorg. Chem. 2024, 63, 18992−19001

interaction and the successive adsorption of gold from aqueous solutions.

Tests for Gold Recovery. To evaluate the capture properties of HS-SWCNT-BP and **$CaZn_6$MethMecys@HS-SWCNT-BP** under static conditions, we first performed an initial screening using an aqueous solution (volume, 400 mL) with an initial Au^{3+} concentration of 5 ppm and testing different pH values (4 and 6). pH values lower than 4 were not tested since the stability of the MOF decreases in an acidic environment, while at pH > 6, mixed Au(III) chloride−hydroxide complexes dominate, which can affect the solubility of gold metal ions.[53] No MTV-BioMOF leaching was observed during the adsorption tests as a result of the stable interactions occurring between the MTV-BioMOF nanocrystals and the SWCNTs.

In the investigated range, we found that pH moderately affects the adsorption performance. The recovery efficiency (RE%) for gold metal ion by the neat HS-SWCNT-BP and the **$CaZn_6$MethMecys@HS-SWCNT-BP** during soaking in aqueous solutions of 5 ppm Au^{3+} at pH values of 4 and 6 in the 0−48 h interval is reported in Figure 3 (Tables S3 and S4, Supporting Information), showing that there is a modest difference among the tested pH conditions: HS-SWCNT-BPs and **$CaZn_6$MethMecys@HS-SWCNT-BP** are able to recover up to 96.3 and 99.5% of gold at pH 4, while the corresponding values at pH = 6 are 85.7 and 90.8%, respectively. A faster adsorption can be noticed for the **$CaZn_6$MethMecys@HS-SWCNT-BP** at pH 4, with the Au^{3+} concentration dropping to 48.6 ppb in less than 16 h (the corresponding concentration at pH 6 being 773.7 ppb, more than 15 times higher), then reaching 34.1 ppb in 24 h, and a final value of 23.9 ppb in 48 h. According to these results, we selected a pH value of 4 for the successive tests.

In addition, it is evident that the presence of the MTV-BioMOFs within the BP slightly increases the final removal efficiency of the neat SWCNT-BP at the tested pH for this selected concentration but significantly improves the adsorption kinetics. Indeed, the residual gold concentrations measured after 16 and 24 h when using the neat HS-SWCNT-BP at pH 4 were 612.8 and 373.4 ppb, respectively, which are more than 10 times higher when compared with the previously reported values for the **$CaZn_6$MethMecys@HS-SWCNT-BP**.

Additional experiments were conducted by increasing the initial nominal concentration of the gold solution at 50 and 100 ppm (Figure 4a, Figure S12, and Tables S5 and S6, Supporting Information). When the concentration of the metal ion increases, the active contribution of the MTV-BioMOF to enhancing the adsorption capacity of the composite material is more evident, even if the overall recovery efficiency value decreases to 68.1 and 76.2% for the HS-SWCNT-BP and the **$CaZn_6$MethMecys@HS-SWCNT-BP**, respectively, for an initial concentration of 50 ppm and to 51.5 and 60.2% when the concentration is further increased to 100 ppm. At this concentration, HS-SWCNT-BP and **$CaZn_6$MethMecys@HS-SWCNT-BP** exhibit maximum adsorption capacities of about 510 and 600 $mg \cdot g^{-1}$, respectively, with an increase of 18% observed for **$CaZn_6$MethMecys@HS-SWCNT-BP** with respect to neat HS-SWCNT-BP. These results indicate that the presence of the MTV-BioMOF **$CaZn_6$MethMecys** within **$CaZn_6$MethMecys@HS-SWCNT-BP** increases the recovery efficiency of the neat HS-SWCNT-BP membrane.

A direct comparison of the efficiency of **$CaZn_6$MethMecys@HS-SWCNT-BP** with other reported functional MOF-based adsorbents is not evident since adsorption tests are performed under different conditions and, in particular, using different initial Au(III) concentrations and adsorbent amounts. However, it can be observed that the maximum adsorption capacity showed by the **$CaZn_6$MethMecys@HS-SWCNT-BP** at the initial Au(III) concentration of 100 ppm compares well to, and even exceeds in some cases, the values recently observed for other functionalized MOFs used as a polycrystalline powder (see Table 1). This result is even more significant if we consider

Table 1. Comparison of Au(III) Adsorption Capacity for Some Adsorbent Materials

material	Au(III) initial concentration (mg/L)	Au(III) adsorption capacity (mg/g)	ref.
MOF microcrystalline powder			
mercapto-1,3,4-thiodiazole Zr-MOF	600	301.5	23
S,N-rich MOF	93	375	55
thiol-decorated MOF-808	98.5	197	56
$CaCu_6$Meth BioMOF	20	598	28
$CaZn_6$MethMecys BioMOF	20	628	this work
MOF-based composites and functional materials			
MOF/poly(thioctic acid) composite	1800	920	57
Ni(II)-pyrazolate−polymer composite, BUT-33−poly(*para*-phenylenediamine)	5000	1600	54
Cu-pPDT MOF 3D functional graphene foam	200	362.2	58
MWCNTs	200	77.5	59
polythiosemicarbazide membrane	1000	523.3	48
$CaZn_6$MethMecys@HS-SWCNT-BP	100	600	this work

that the **$CaZn_6$MethMecys@HS-SWCNT-BP** is a composite material, for which lower adsorption capacity values are expected due to a reduced accessibility of the MOF pores as a result of its inclusion in a support matrix.[54] Moreover, the maximum adsorption capacity of **$CaZn_6$MethMecys@HS-SWCNT-BP** is also comparable to that of other recently reported functional or composite materials, also by taking into account that usually higher initial Au(III) concentrations, from 2 up to 50 times higher, have been used.

The higher removal efficiency of **the $CaZn_6$MethMecys@HS-SWCNT-BP** composite with respect to the neat HS-SWCNT-BP can be directly attributed to the presence of the MTV-BioMOF, which displays a superior affinity for gold metal ions. Considering the single-crystal X-ray structural determination of the MTV-BioMOF **$CaZn_6$MethMecys**, it is evident that two types of flexible and cooperative thioalkyl groups, decorating the hexagonal MOF channels, afford an adaptable functional environment, which boosts the interactions with gold metal ions by exploiting the well-known affinity of S atoms for gold.

Since gold is often present in complex water matrices along with other interfering species including competing metal ions and organic molecules, we also tested the selectivity of the **$CaZn_6$MethMecys@HS-SWCNT-BP** for gold extraction in the presence of other commonly occurring metal ions, i.e.,

https://doi.org/10.1021/acs.inorgchem.4c03407
Inorg. Chem. 2024, 63, 18992−19001

silver(I), nickel(II), and cobalt(II) (Figure 4b and Tables S7, Supporting Information). Thus, we prepared a multi-ion aqueous solution containing all these metals at an initial concentration of 3 ppm at pH = 4. The RE% for gold maintained a very high value of 98.0%. The most competing metal cation was Ag(I) (67.3%) followed by Ni(II) (51.9%) and Co(II) (49.2%).

The gold distribution coefficients, K_D, between the **CaZn$_6$MethMecys@HS-SWCNT-BP** and the solutions both in the 5 ppm pure gold solution and the 3 ppm multi-component (Au, Ag, Ni, and Co) solution were calculated according to the following equation:[60]

$$K_D = \frac{[Au^{3+}]_{BP}}{[Au^{3+}]_{sol}} \quad (1)$$

where $[Au]^{3+}_{BP}$ (mg·kg^{-1}) and $[Au]^{3+}_{sol}$ (mg·L^{-1}) are the gold ion concentrations at equilibrium adsorbed onto the **CaZn$_6$MethMecys@HS-SWCNT-BP** and present in the solution, respectively. Generally, a value of log K_D larger than 5 is indicative of a high affinity of an ion for a substrate and suggests that the ion is likely adsorbed. The values for log K_D for the HS-SWCNT-BP and the **CaZn$_6$MethMecys@HS-SWCNT-BP** in the 5 ppm gold solution are 4.1 and 6.0 respectively, confirming the increased affinity of gold for the BioMOF-decorated HS-SWCNT-BP. The respective value calculated for the **CaZn$_6$MethMecys@HS-SWCNT-BP** for the 3 ppm multi-ion solution is 5.5, indicating that the superior affinity of gold for the composite material is preserved even in the presence of interfering ions.

Au(III) adsorption curves for **CaZn$_6$MethMecys@HS-SWCNT-BP** and HS-SWCNT-BP have been fitted assuming that the gold adsorption process can be described by the Lagergren first-order equation:[61,62]

$$\frac{dq_t}{dt} = k_1(q_e - q_t) \quad (2)$$

where q_t and q_e are respectively the Au adsorption capacity per unit of adsorbent mass (mg·g^{-1}) at time t and at equilibrium and k_1 is the Lagergren adsorption rate constant (min^{-1}). The experimental amount q_t is calculated as follows:

$$q_t = \frac{(C_0 - C_t)V}{m} \quad (3)$$

with C_0 and C_t being the gold concentration at time t = 0 and time t, respectively, m the adsorbent mass (g) (i.e., the mass of BPs), and V the volume of gold solutions.

By integration, eq 2 becomes

$$q_t = q_e(1 - e^{-kt}) \quad (4)$$

OriginPro 2019 software has been used to fit experimental adsorption data as a function of time.[63] The nonlinear optimization method by Origin software was used instead of linear regression to avoid any distortions created in the original error distribution.[64]

The calculated Lagergren adsorption rate constants at initial Au concentrations of 5 and 50 ppm are reported in Table 2.

The Lagergren first-order equation fitting properly matches the behavior observed experimentally, confirming that the incorporation of **CaZn$_6$MethMecys** MTV) BioMOF in HS-SWCNT-BPs greatly enhances their performance in the adsorption of gold from aqueous solutions. The calculated

Table 2. Lagergren Adsorption Rate Constants k_1 (min^{-1}) at 5 and 50 ppm Initial Au Concentrations

	CaZn$_6$MethMecys@HS-SWCNT-BP	neat HS-SWCNT-BP
5 ppm	0.0099 ± 0.0007	0.0064 ± 0.0007
50 ppm	0.0095 ± 0.0009	0.0071 ± 0.0006

Lagergren adsorption rate constants at the initial Au concentrations of 5 and 50 ppm for HS-SWCNTs-BPs were 0.0064 ± 0.0007 and 0.0071 ± 0.0006 min^{-1}, respectively. These values increase by about 55% for **CaZn$_6$MethMecys@HS-SWCNT-BPs**, with values of 0.0099 ± 0.0007 min^{-1} (5 ppm Au) and 0.0095 ± 0.0009 min^{-1} (50 ppm Au).

In addition, since an efficient adsorbent material should be stable over long-term use, maintaining high gold capacity and removal efficiency in several cycles of use, we demonstrated the recycling ability of the **CaZn$_6$MethMecys@HS-SWCNT-BP** after its reuse in successive adsorption tests. Sorption experiments were repeated alternating with a regeneration step with 250 mL of mercaptoethanol/water solution with a 1:9 ratio. The composite material maintained its scavenging ability after three cycles (Figure 5 and Table S8), with a minor loss of the original adsorption capacity (<5%).

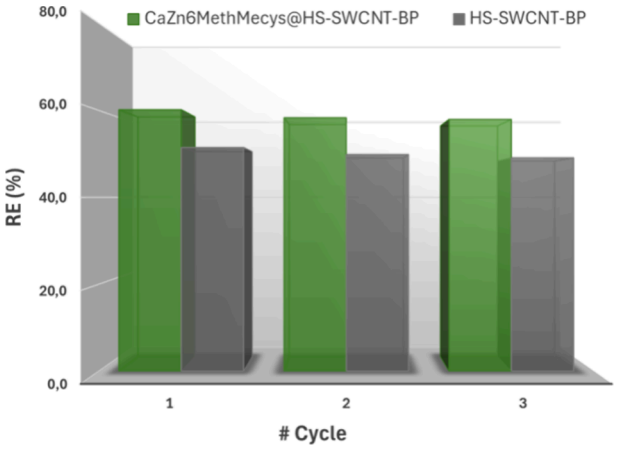

Figure 5. Recovery efficiency (RE%) for gold metal ion of **CaZn$_6$MethMecys@HS-SWCNT-BP** and HS-SWCNT-BP during soaking in aqueous solutions of 100 ppm gold (volume, 400 mL) at pH 4.

CONCLUSIONS

In this study, a composite **CaZn$_6$MethMecys@HS-SWCNT-BP** membrane loaded with an MTV-BioMOFs was successfully prepared via simple mixing and filtration. The presence of the MTV-BioMOFs (**1**) assured highly efficient gold metal ion adsorption from water, even in the presence of other competing metal ions. The enhanced adsorption performance of **CaZn$_6$MethMecys@HS-SWCNT-BP** with respect to HS-SWCNT-BP can be mainly attributed to the functional microenvironment of the MTV-BioMOF, as the thioalkyl groups of the natural amino acid residues from both the methyl cysteine- and methionine-derived ligands provide convenient recognition sites for metal adsorption. A highly efficient gold removal was observed even in the presence of competing ions, i.e., silver, cobalt, and nickel, with a good selectivity. It is likely that the thioether groups of the amino acid residues establish preferential interactions with the Au^{3+} ions and, to a minor

https://doi.org/10.1021/acs.inorgchem.4c03407
Inorg. Chem. 2024, 63, 18992−19001

extent, with the Ag^+, Ni^{2+}, and Co^{2+} cations, through the sulfur atom. Furthermore, the successful regeneration to remove the adsorbed metals makes these membranes promising candidates for practical application in the selective extraction and enrichment of gold as well as for water remediation.

EXPERIMENTAL SECTION

Chemicals. All chemicals were of reagent-grade quality. They were purchased from commercial sources and used as received. SWCNTs (characterized by an average diameter of 1.4 ± 0.1 nm and an average length longer than 5 μm, as reported in the datasheet from Sigma-Aldrich, Milan, Italy) were used for the preparation of SWCNT dispersions and synthesis of HS-SWCNTs. Compound $\{Ca^{II}Zn^{II}_6[(S,S)\text{-methox}]_{1.5}[(S,S)\text{-mecysmox}]_{1.50}(OH)_2(H_2O)\}\cdot xH_2O$ (**1**) MTV-BioMOF was prepared as reported earlier for a similar MTV-MOF containing Cu(II).[38]

Physical Techniques. Elemental (C, H, S, and N) analyses were performed at the Microanalytical Service of the Universitat de València. FT-IR spectra were recorded on a PerkinElmer 882 spectrophotometer as KBr pellets. Thermogravimetric analysis (TGA) data were recorded on an SDT-Q600 analyzer from TA Instruments. The temperature varied from RT to 490 °C at a heating rate of 10 °C min^{-1}. Measurements were carried out on samples in open platinum crucibles under a flow of air.

X-ray Powder Diffraction Measurements. A polycrystalline sample of **$CaZn_6$MethMecys** was introduced into a 0.5 mm borosilicate capillary prior to being mounted and aligned on a Bruker D8 Discover powder diffractometer using Cu Kα radiation (λ = 1.54056 Å). For each sample, five repeated measurements were collected at room temperature (2θ = 3−60°) and merged in a single diffractogram.

Gas Adsorption. The N_2 adsorption−desorption at 77 K was carried out on a polycrystalline sample of **$CaZn_6$MethMecys** with a BELSORP-miniX instrument. The sample was first activated with methanol and then evacuated at 348 K during 19 h under 10^{-6} Torr prior to the analysis.

Synthesis of $\{Ca^{II}Zn^{II}_6[(S,S)\text{-Methox}]_{1.5}[(S,S)\text{-mecysmox}]_{1.50}(OH)_2(H_2O)\}\cdot 12H_2O$ (CaZn$_6$MethMecys). H_2Me_2-(*S*,*S*)-Mecysmox (2.11 g, 6.0 mmol) and H_2Me_2-(S,S)-methox (2.34 g, 6.0 mmol) ligands were suspended in 80 mL of water and treated with a 25% methanolic solution of Me_4NOH (14.5 mL, 50.0 mmol) until complete dissolution. Then, another aqueous solution (40 mL) containing $CaCl_2$ (0.45 g, 4.0 mmol) and $Zn(NO_3)6H_2O$ (6.98 g, 24.0 mmol) was added dropwise under stirring. After further stirring for 10 h, at room temperature, a white polycrystalline powder was obtained and collected via filtration and dried with methanol. Well-shaped hexagonal prisms of **$CaZn_6$MethMecys** suitable for X-ray structural analysis could be obtained by slow diffusion, in an H-shaped tube, of aqueous solutions containing stoichiometric amounts of H_2Me_2-(*S*,*S*)-Mecysmox (0.010 g, 0.06 mmol), H_2Me_2-(*S*,*S*)-methox (0.011 g, 0.06 mmol) and Me_4NOH (0.72 mL, 2.5 mmol) in one arm and $CaCl_2$ (0.021 g, 0.2 mmol) and $Zn(NO_3)\cdot 6H_2O$ (0.035 g, 0.12 mmol) in the other. They were isolated by filtration on paper and air-dried. Anal. for **$CaZn_6$MethMecys**, $C_{33}Zn_6CaS_6H_{70}N_6O_{33}$ (1703.74): C, 23.26; H, 4.14; S, 11.29; N, 4.93%. Found: C, 23.31; H, 4.13; S, 11.31; N, 4.99%; IR (KBr): ν = 1625 and 1596 cm^{-1} (C═O).

Synthesis of HS-SWCNTs. In a 500 mL three-neck round-bottom flask equipped with a UP400S powerful ultrasonicator (Hielscher) and under a nitrogen atmosphere, 0.3 g of SWCNTs (Sigma-Aldrich, cod. 805033) and 1.2 g of S_8 (Sigma-Aldrich, cod. 213292) in dry acetone (100 mL) were placed. The suspension was sonicated for 3 h using a 60% amplitude and 0.5 cycles. Subsequently, the dispersion was subjected to UV irradiation under a UV lamp (Oriel Instruments, model 66922) using the following program: 1000 W for 20 min and 800 W for 20 min. The obtained material was filtered through a sintered PTFE filter and dried under vacuum. The obtained dark powder was subjected to Soxhlet extraction for 48 h using 150 mL of acetone and dried under vacuum to give a sulfurated CNTs powder (SS-SWCNTs).

In a 250 mL three-neck round-bottom flask, equipped with a magnetic stir bar, under a nitrogen atmosphere, sulfurated CNTs were suspended in dry ethanol (100 mL). The system was placed in an ultrasound bath (Branson 1510 ultrasonic cleaner), and $NaBH_4$ was added portionwise for 30 min under stirring. The reaction was conducted at room temperature for 3 h under sonication. A reduced CNTs (HS-SWCNTs) dispersion was filtered through a sintered PTFE filter, washed with ethanol (5 mL × 4), and dried under vacuum to give the desired product as a black powder. All solvents were purchased from Sigma-Aldrich.

Preparation of HS-SWCNT-BPs. After sonication (5 h) in an ultrasonic bath (model M1800H-E, Bransonic, Danbury, CT, USA), a methanol dispersion of HS-SWCNTs (40 mg) was filtered under vacuum (pressure = −0.04 bar) through a PTFE filter and then dried at room temperature. **$CaZn_6$MethMecys@HS-SWCNT-BP** membranes were obtained following the same procedure above-described. The MTV-BioMOF and the HS-SWCNTs, weight ratio of 25%:75%, were dispersed in 150 mL of methanol; then, the dispersion was filtered under vacuum, and after drying, the obtained membrane was peeled off from PTFE filter. The filtered solution was analyzed with ICP-MS, proving that the MOF was retained in the formed buckypaper. Both membrane topologies (HS-SWCNT-BP and **$CaZn_6$MethMecys@HS-SWCNT-BP**) are circular, self-standing flexible disks, with an average diameter of 38 ± 1 mm.

X-ray Crystallographic Data Collection and Structure Refinement. A suitable crystal of **$CaZn_6$MethMecys** with ca. 0.16 mm × 0.10 mm × 0.10 mm as dimensions was selected and mounted on a MITIGEN holder in Paratone oil. Then, it was very quickly placed on a nitrogen stream cooled at 220 K to avoid possible degradation upon dehydration. Diffraction data were collected on a Bruker-Nonius X8APEXII CCD area detector diffractometer using graphite-monochromated Mo Kα radiation (λ = 0.71073 Å). Further crystallographic details can be found in the Supporting Information.

FT-IR Spectroscopy. FT-IR spectra were recorded on a Fourier transform infrared (FT-IR) spectrometer (Bruker ALPHA FT-IR) equipped with a A241/D reflection module. The spectra were collected in the region of 375−4000 cm^{-1} and interpreted with OPUS Bruker software. The FT-IR spectra are shown in Figure S6.

XPS Spectroscopy. XPS measurements were conducted using an Al Kα X-ray source in an ultrahigh vacuum chamber with a base pressure of 1 × 10^{-9} Torr. Pristine SWCNT and HS-SWCNT buckypaper samples were mounted on grounded conductive glass substrates. Spectra were taken with a semihemispherical energy analyzer working in a constant pass energy mode (100 eV) and corrected for the transmission factor. Further details can be found in the Supporting Information.

Raman Spectroscopy. Raman analyses were performed by using a confocal micro-Raman LABRAM supplied by Horiba-Jobin-Yvon equipped with a Nd:YAG laser at 532 nm, a charge-coupled device (CCD) cooled with a Peltier module 1024 × 256, a 16-bit dynamic range (pixel size, 27 μm), and a long working distance objective of 50×. Further details can be found in the Supporting Information.

Scanning Electron Microscopy. SEM measurements were carried out using a LEO 420 scanning electron microscope (SEM, Zeiss) (vacuum conditions: 1 × 10^{-6} Torr, accelerating voltage: 15 kV) coupled with an energy-dispersive X-ray (EDX) detector (INCAx-Sight, Oxford Instruments). EDX measurements were recorded at the following conditions: iProbe, 650 pA; vacuum, 1 × 10^{-6} Torr; current filament, 15 kV. Further details can be found in the Supporting Information.

Adsorption Experiments. Au adsorption was evaluated for both HS-SWCNT-BP and **$CaZn_6$MethMecys@HS-SWCNT-BP**. ICP-MS analyses for the Au capture experiments with the membrane were performed at the Department of Chemistry of the University of Calabria to determine the residual metal concentration and to assess the eventual presence of leached MOF in the solution. Experiments were performed by placing 1 disk with a diameter of 38 mm in 400 mL of $HAuCl_4$ aqueous solutions (1000 ppm, 7% HCl, supplied by Sigma-Aldrich), and adsorption was evaluated at the following Au

https://doi.org/10.1021/acs.inorgchem.4c03407
Inorg. Chem. 2024, 63, 18992−19001

concentrations: 5, 50, and 100 ppm. Further details can be found in the Supporting Information.

Mechanical Properties. Tensile strength measurements on both HS-SWCNT-BP and **$CaZn_6$MethMecys@HS-SWCNT-BP** were performed through a Sauter TVO-S tensile tester equipped with a Sauter FH-1k digital dynamometer and AFH FAST software (Sauter GmbH, Balingen, Germany). Samples were cut in rectangular strips (width of 5 mm and length of 30 mm) and tested at a strain rate of 0.1 mm min^{-1}.

■ ASSOCIATED CONTENT

Supporting Information

The Supporting Information is available free of charge at https://pubs.acs.org/doi/10.1021/acs.inorgchem.4c03407.

Additional experimental details and physical and analytical characterization data for **$CaZn_6$MethMecys** and **$CaZn_6$MethMecys@HS-SWCNT-BP** with crystallographic refinement details for **$CaZn_6$MethMecys** (Figures S1 and S2 and Tables S1−S8) (PDF)

Accession Codes

CCDC 2373286 contains the supplementary crystallographic data for this paper. These data can be obtained free of charge via www.ccdc.cam.ac.uk/data_request/cif, or by emailing data_request@ccdc.cam.ac.uk, or by contacting The Cambridge Crystallographic Data Centre, 12 Union Road, Cambridge CB2 1EZ, UK; fax: +44 1223 336033.

■ AUTHOR INFORMATION

Corresponding Authors

Emilio Pardo − *Department of Inorganic Chemistry/Institute of Molecular Science, University of Valencia Paterna, Valencia 46980, Spain;* orcid.org/0000-0002-1394-2553; Email: emilio.pardo@uv.es

Giovanni De Filpo − *Department of Chemistry and Chemical Technologies, University of Calabria, Rende 87036, Italy;* Email: defilpo@unical.it

Donatella Armentano − *Department of Chemistry and Chemical Technologies, University of Calabria, Rende 87036, Italy;* orcid.org/0000-0002-8502-8074; Email: donatella.armentano@unical.it

Authors

Mariafrancesca Baratta − *Department of Chemistry and Chemical Technologies, University of Calabria, Rende 87036, Italy;* orcid.org/0000-0002-9966-8312

Teresa F. Mastropietro − *Department of Chemistry and Chemical Technologies, University of Calabria, Rende 87036, Italy*

Paula Escamilla − *Department of Inorganic Chemistry/Institute of Molecular Science, University of Valencia Paterna, Valencia 46980, Spain*

Vincenzo Algieri − *IRCCS NEUROMED-Istituto Neurologico Mediterraneo, Pozzilli (IS) 86077, Italy;* orcid.org/0000-0002-1163-8072

Fang Xu − *Department of Biology, Ecology and Earth Science University of Calabria, Rende 87036, Italy*

Fiore Pasquale Nicoletta − *Department of Pharmacy, Health and Nutritional Sciences University of Calabria, Rende 87036, Italy*

Jesus Ferrando-Soria − *Department of Inorganic Chemistry/Institute of Molecular Science, University of Valencia Paterna, Valencia 46980, Spain*

Complete contact information is available at: https://pubs.acs.org/10.1021/acs.inorgchem.4c03407

Author Contributions

[#]M.B. and T.F.M. have equally contributed to this work. The manuscript was written through contributions of all authors. All authors have given approval to the final version of the manuscript.

Notes

The authors declare no competing financial interest.

■ ACKNOWLEDGMENTS

This work was supported by the Ministero dell'Istruzione, dell'Università e della Ricerca (Italy) and the MICINN (Spain) (Project PID2022-136349OB-I00 and Excellence Unit "Maria de Maeztu" CEX2019-000919-M). D.A. also acknowledges financial support of the European Union−NextGenerationEU under the National Recovery and Resilience Plan (NRRP) of Ministero dell'Università e della Ricerca (MUR) (Project code PE0000021, "Network 4 Energy Sustainable Transition−NEST). Thanks are also extended to the "Generalitat Valenciana" (Project PROMETEO/2021/054). E.P. acknowledges financial support of the European Research Council under the European Union's Horizon 2020 research and innovation program/ERC Grant Agreement No. 814804, MOF−reactors. Thanks are also extended to the Ramón y Cajal Program, RYC2019-027940-I (J.F.-S.). This study forms part of the Advanced Materials program (MFA/2022/048) and was supported by MCIN with funding from European Union NextGenerationEU (PRTR-C17.I1) and by Generalitat Valenciana.

■ ABBREVIATIONS

MTV-BioMOF, multivariate biological metal−organic framework; SWCNT-BP, single-walled carbon nanotube buckypapers; MWCNTs, multiwalled carbon nanotubes

■ REFERENCES

(1) Forti, V.; Balde, C. P.; Kuehr, R.; Bel, G. *The Global E-waste Monitor 2020: Quantities, flows and the circular economy potential*; United Nations University (UNU), International Telecommunication Union (ITU) & International Solid Waste Association (ISWA): Bonn/Geneva/Rotterdam, 120.

(2) Baldé, C. P.; Forti, V.; Gray, V.; Kuehr, R.; Stegmann, P. *The Global E-Waste Monitor 2017: Quantities, Flows, and Resources*; International Telecommunication Union: 2017.

(3) Schluep, M.; Hagelüken, C.; Kuehr, R.; Magalini, F. *Recycling-from e-Waste to Resources*; United Nations Environmental Program (UNEP) & United Nations University (UNU): 2009. https://www.researchgate.net/publication/278849195.

(4) Gurung, M.; Adhikari, B. B.; Kawakita, H.; Ohto, K.; Inoue, K.; Alam, S. Selective Recovery of Precious Metals from Acidic Leach Liquor of Circuit Boards of Spent Mobile Phones Using Chemically Modified Persimmon Tannin Gel. *Ind. Eng. Chem. Res.* **2012**, *51* (37), 11901−11913.

(5) Yue, C.; Sun, H.; Liu, W.; Guan, B.; Deng, X.; Zhang, X.; Yang, P. Environmentally Benign, Rapid, and Selective Extraction of Gold from Ores and Waste Electronic Materials. *Angew. Chem.* **2017**, *129* (32), 9459−9463.

(6) Nguyen, N. V.; Jeong, J.; Shin, D.; Kim, B. S.; Lee, J. C.; Pandey, B. D. Simultaneous Recovery of Gold and Iodine from the Waste Rinse Water of the Semiconductor Industry Using Activated Carbon. *Mater. Trans.* **2012**, *53*, 760−765.

(7) Yap, C. Y.; Mohamed, N. An Electrogenerative Process for the Recovery of Gold from Cyanide Solutions. *Chemosphere* **2007**, *67* (8), 1502−1510.

(8) Syed, S. Recovery of Gold from Secondary Sources-A Review. *Hydrometallurgy* **2012**, *115-116*, 30−51.
(9) Ankit; Saha, L.; Kumar, V.; Tiwari, J.; Sweta; Rawat, S.; Singh, J.; Bauddh, K. Electronic Waste and Their Leachates Impact on Human Health and Environment: Global Ecological Threat and Management. *Environ. Technol. Innovation* **2021**, *24*, No. 102049.
(10) Rao, M. D.; Singh, K. K.; Morrison, C. A.; Love, J. B. Challenges and Opportunities in the Recovery of Gold from Electronic Waste. *RSC Adv.* **2020**, *10* (8), 4300−4309.
(11) Do, M. H.; Nguyen, G. T.; Thach, U. D.; Lee, Y.; Bui, T. H. Advances in Hydrometallurgical Approaches for Gold Recovery from E-Waste: A Comprehensive Review and Perspectives. *Miner. Eng.* **2023**, *191*, No. 107977.
(12) Nogueira, A. F. M.; Carreira, A. R. F.; Vargas, S. J. R.; Passos, H.; Schaeffer, N.; Coutinho, J. A. P. Simple Gold Recovery from E-Waste Leachate by Selective Precipitation Using a Quaternary Ammonium Salt. *Sep. Purif. Technol.* **2023**, *316*, No. 123797.
(13) Xing, W. D.; Lee, M. S.; Kim, Y. H. Separation of Gold(III) from Hydrochloric Acid Solution Containing Platinum(IV) and Palladium(II) by Solvent Extraction with Cyanex 272 and LIX 63. *Journal of Industrial and Engineering Chemistry* **2018**, *59*, 328−334.
(14) Murakami, H.; Nishihama, S.; Yoshizuka, K. Separation and Recovery of Gold from Waste LED Using Ion Exchange Method. *Hydrometallurgy* **2015**, *157*, 194−198.
(15) Parinayok, P.; Yamashita, M.; Yonezu, K.; Ohashi, H.; Watanabe, K.; Okaue, Y.; Yokoyama, T. Interaction of Au(III) and Pt(IV) Complex Ions with Fe(II) Ions as a Scavenging and a Reducing Agent: A Basic Study on the Recovery of Au and Pt by a Chemical Method. *J. Colloid Interface Sci.* **2011**, *364* (1), 272−275.
(16) Xie, F.; Fan, Z.; Zhang, Q.; Luo, Z. Selective Adsorption of Au3+ from Aqueous Solutions Using Persimmon Powder-Form-aldehyde Resin. *J. Appl. Polym. Sci.* **2013**, *130* (6), 3937−3946.
(17) Xiong, C.; Li, Y.; Wang, S.; Zhou, Y. Functionalization of Nanosilica via Guanidinium Ionic Liquid for the Recovery of Gold Ions from Aqueous Solutions. *J. Mol. Liq.* **2018**, *256*, 183−190.
(18) Ghorbani-Kalhor, E.; Behbahani, M.; Abolhasani, J. Application of Ion-Imprinted Polymer Nanoparticles for Selective Trace Determination of Palladium Ions in Food and Environmental Samples with the Aid of Experimental Design Methodology. *Food Anal Methods* **2015**, *8* (7), 1746−1757.
(19) Zhou, H. C.; Long, J. R.; Yaghi, O. M. Introduction to Metal-Organic Frameworks. *Chem. Rev.* **2012**, *112*, 673−674.
(20) Chen, J. Q.; Sharifzadeh, Z.; Bigdeli, F.; Gholizadeh, S.; Li, Z.; Hu, M. L.; Morsali, A. MOF Composites as High Potential Materials for Hazardous Organic Contaminants Removal in Aqueous Environments. *J. Environ. Chem. Eng.* **2023**, *11*, No. 109469.
(21) Mon, M.; Bruno, R.; Ferrando-Soria, J.; Armentano, D.; Pardo, E. Metal-Organic Framework Technologies for Water Remediation: Towards a Sustainable Ecosystem. *Journal of Materials Chemistry A* **2018**, *6*, 4912−4947.
(22) Cohen, S. M. Postsynthetic Methods for the Functionalization of Metal-Organic Frameworks. *Chem. Rev.* **2012**, *112*, 970−1000.
(23) Wang, C.; Lin, G.; Zhao, J.; Wang, S.; Zhang, L. Enhancing Au(III) Adsorption Capacity and Selectivity via Engineering MOF with Mercapto-1,3,4-Thiadiazole. *Chem. Eng. J.* **2020**, *388*, No. 124221.
(24) Ma, Q.; Zhang, T.; Wang, B. Shaping of Metal-Organic Frameworks, a Critical Step toward Industrial Applications. *Matter.* **2022**, *5*, 1070−1091.
(25) Liu, X. M.; Xie, L. H.; Wu, Y. Recent Advances in the Shaping of Metal-Organic Frameworks. *Inorganic Chemistry Frontiers.* **2020**, *7*, 2840−2866.
(26) Wang, H.; Zhao, S.; Liu, Y.; Yao, R.; Wang, X.; Cao, Y.; Ma, D.; Zou, M.; Cao, A.; Feng, X.; Wang, B. Membrane Adsorbers with Ultrahigh Metal-Organic Framework Loading for High Flux Separations. *Nat. Commun.* **2019**, *10* (1), 4204.
(27) Zhang, Y.; Feng, X.; Li, H.; Chen, Y.; Zhao, J.; Wang, S.; Wang, L.; Wang, B. Photoinduced Postsynthetic Polymerization of a Metal−Organic Framework toward a Flexible Stand-Alone Membrane. *Angew. Chem.* **2015**, *127* (14), 4333−4337.
(28) Mon, M.; Ferrando-Soria, J.; Grancha, T.; Fortea-Pérez, F. R.; Gascon, J.; Leyva-Pérez, A.; Armentano, D.; Pardo, E. Selective Gold Recovery and Catalysis in a Highly Flexible Methionine-Decorated Metal-Organic Framework. *J. Am. Chem. Soc.* **2016**, *138* (25), 7864−7867.
(29) Mon, M.; Lloret, F.; Ferrando-Soria, J.; Martí-Gastaldo, C.; Armentano, D.; Pardo, E. Selective and Efficient Removal of Mercury from Aqueous Media with the Highly Flexible Arms of a BioMOF. *Angew. Chem.* **2016**, *128* (37), 11333−11338.
(30) Helal, A.; Yamani, Z. H.; Cordova, K. E.; Yaghi, O. M. Multivariate Metal-Organic Frameworks. *Natl. Sci. Rev.* **2017**, *4* (3), 296−298.
(31) Kong, X.; Deng, H.; Yan, F.; Kim, J.; Swisher, J. A.; Smit, B.; Yaghi, O. M.; Reimer, J. A. Mapping of Functional Groups in Metal-Organic Frameworks. *Science (1979)* **2013**, *341* (6148), 882−885.
(32) Zhang, Y. B.; Furukawa, H.; Ko, N.; Nie, W.; Park, H. J.; Okajima, S.; Cordova, K. E.; Deng, H.; Kim, J.; Yaghi, O. M. Introduction of Functionality, Selection of Topology, and Enhancement of Gas Adsorption in Multivariate Metal-Organic Framework-177. *J. Am. Chem. Soc.* **2015**, *137* (7), 2641−2650.
(33) Deng, H.; Doonan, C. J.; Furukawa, H.; Ferreira, R. B.; Towne, J.; Knobler, C. B.; Wang, B.; Yaghi, O. M. Multiple Functional Groups of Varying Ratios in Metal-Organic Frameworks. *Science (1979)* **2010**, *327* (5967), 846−850.
(34) Mon, M.; Bruno, R.; Tiburcio, E.; Viciano-Chumillas, M.; Kalinke, L. H. G.; Ferrando-Soria, J.; Armentano, D.; Pardo, E. Multivariate Metal-Organic Frameworks for the Simultaneous Capture of Organic and Inorganic Contaminants from Water. *J. Am. Chem. Soc.* **2019**, *141* (34), 13601−13609.
(35) Viciano-Chumillas, M.; Liu, X.; Leyva-Pérez, A.; Armentano, D.; Ferrando-Soria, J.; Pardo, E. Mixed Component Metal-Organic Frameworks: Heterogeneity and Complexity at the Service of Application Performances. *Coord. Chem. Rev.* **2022**, *451*, No. 214273.
(36) Bruno, R.; Mon, M.; Escamilla, P.; Ferrando-Soria, J.; Esposito, E.; Fuoco, A.; Monteleone, M.; Jansen, J. C.; Elliani, R.; Tagarelli, A.; Armentano, D.; Pardo, E. Bioinspired Metal-Organic Frameworks in Mixed Matrix Membranes for Efficient Static/Dynamic Removal of Mercury from Water. *Adv. Funct. Mater.* **2021**, *31* (6), 2008499.
(37) Tursi, A.; Mastropietro, T. F.; Bruno, R.; Baratta, M.; Ferrando-Soria, J.; Mashin, A. I.; Nicoletta, F. P.; Pardo, E.; De Filpo, G.; Armentano, D. Synthesis and Enhanced Capture Properties of a New BioMOF@SWCNT-BP: Recovery of the Endangered Rare-Earth Elements from Aqueous Systems. *Adv. Mater. Interfaces* **2021**, *8* (16), 2100730.
(38) Baratta, M.; Mastropietro, T. F.; Bruno, R.; Tursi, A.; Negro, C.; Ferrando-Soria, J.; Mashin, A. I.; Nezhdanov, A.; Nicoletta, F. P.; De Filpo, G.; Pardo, E.; Armentano, D. Multivariate Metal-Organic Framework/Single-Walled Carbon Nanotube Buckypaper for Selective Lead Decontamination. *ACS Appl. Nano Mater.* **2022**, *5* (4), 5223−5233.
(39) Dubey, R.; Dutta, D.; Sarkar, A.; Chattopadhyay, P. Functionalized Carbon Nanotubes: Synthesis, Properties and Applications in Water Purification, Drug Delivery, and Material and Biomedical Sciences. *Nanoscale Advances.* **2021**, *3*, 5722−5744.
(40) Gholami, S.; López, J.; Rezvani, A.; Vatanpour, V.; Cortina, J. L. Fabrication of Thin-Film Nanocomposite Nanofiltration Membranes Incorporated with Aromatic Amine-Functionalized Multiwalled Carbon Nanotubes. Rejection Performance of Inorganic Pollutants from Groundwater with Improved Acid and Chlorine Resistance. *Chem. Eng. J.* **2020**, *384*, No. 123348.
(41) Rashid, M. H. O.; Ralph, S. F. Carbon Nanotube Membranes: Synthesis, Properties, and Future Filtration Applications. *Nanomaterials* **2017**, *7*, 99.
(42) Sarkar, B.; Mandal, S.; Tsang, Y. F.; Kumar, P.; Kim, K. H.; Ok, Y. S. Designer Carbon Nanotubes for Contaminant Removal in Water and Wastewater: A Critical Review. *Sci. Total Environ.* **2018**, *612*, 561−581.

https://doi.org/10.1021/acs.inorgchem.4c03407
Inorg. Chem. 2024, 63, 18992−19001

(43) Baratta, M.; Nezhdanov, A. V.; Mashin, A. I.; Nicoletta, F. P.; De Filpo, G. Carbon Nanotubes Buckypapers: A New Frontier in Wastewater Treatment Technology. *Sci. Total Environ.* **2024**, *924*, No. 171578.
(44) Ralph Pearson, B. G. *PHYSICAL AND INORGANIC CHEMISTRY Hard and Soft Acids and Bases*; UTC, 2024; Vol. *13*. https://pubs.acs.org/sharingguidelines.
(45) Birtane, H.; Urucu, O. A.; Yıldız, N.; Çiğil, A. B.; Kahraman, M. V. Statistical Optimization and Selective Uptake of Au(III) from Aqueous Solution Using Carbon Nanotube-Cellulose Based Adsorbent. *Mater. Today Commun.* **2022**, *30*, No. 103144.
(46) Minati, L.; Speranza, G.; Torrengo, S.; Toniutti, L.; Migliaresi, C.; Maniglio, D.; Ferrari, M.; Chiasera, A. Characterization of Thiol-Functionalized Carbon Nanotubes on Gold Surfaces. *Surf. Sci.* **2010**, *604* (17−18), 1414−1419.
(47) Afrin, R.; Shah, N. A. Room Temperature Gas Sensors Based on Carboxyl and Thiol Functionalized Carbon Nanotubes Buckypapers. *Diam Relat Mater.* **2015**, *60*, 42−49.
(48) Villalobos, L. F.; Yapici, T.; Peinemann, K. V. Poly-Thiosemicarbazide Membrane for Gold Recovery. *Sep Purif Technol.* **2014**, *136*, 94−104.
(49) Rouquerol, J.; Avnir, D.; Fairbridge, C. W.; Everett, D. H.; Haynes, J. M.; Pernicone, N.; Ramsay, J. D. F.; Sing, K. S. W.; Unger, K. K. Recommendations for the Characterization of Porous Solids (Technical Report). *Pure Appl. Chem.* **1994**, *66* (8), 1739−1758.
(50) Cheng, L. S.; Yang, R. T. Improved Horvath—Kawazoe Equations Including Spherical Pore Models for Calculating Micropore Size Distribution. *Chem. Eng. Sci.* **1994**, *49* (16), 2599−2609.
(51) Pan, B.; Xing, B. Adsorption Mechanisms of Organic Chemicals on Carbon Nanotubes. *Environ. Sci. Technol.* **2008**, *42*, 9005−9013.
(52) Mao, J.; Wang, Y.; Zhu, J.; Yu, J.; Hu, Z. Thiol Functionalized Carbon Nanotubes: Synthesis by Sulfur Chemistry and Their Multi-Purpose Applications. *Appl. Surf. Sci.* **2018**, *447*, 235−243.
(53) Usher, A.; McPhail, D. C.; Brugger, J. A Spectrophotometric Study of Aqueous Au(III) Halide-Hydroxide Complexes at 25−80 °C. *Geochim. Cosmochim. Acta* **2009**, *73* (11), 3359−3380.
(54) Xue, T.; He, T.; Peng, L.; Syzgantseva, O. A.; Li, R.; Liu, C.; Sun, D. T.; Xu, G.; Qiu, R.; Wang, Y.; Yang, S.; Li, J.; Li, J.-R.; Queen, W. L. A Customized MOF-Polymer Composite for Rapid Gold Extraction from Water Matrices. *Adv. Sci.* **2023**, *9*, No. eadg4923.
(55) Wang, B.; Ma, Y.; Xu, W.; Tang, K. A Novel S,N-Rich MOF for Efficient Recovery of Au(III): Performance and Mechanism. *J. Hazard. Mater.* **2023**, *451*, No. 131051.
(56) Zhao, X.; Wu, M.; Huang, H.; Liu, B. Dual Thiols-Decorated Metal−Organic Framework for Efficient Separation and Recovery of Gold. *Sep. Purif. Technol.* **2024**, *328*, No. 125127.
(57) Li, R.; Yan, S.; Xue, T.; Qiu, R.; Li, Y.; Hao, W.; Xu, G.; Wang, Y.; Hong, Y.; Su, Y.; Wang, H.; Yang, S.; Peng, L.; Li, J. A MOF/Poly(Thioctic Acid) Composite for Enhanced Gold Extraction from Water Matrices. *Nano Res.* **2024**, *17* (1), 382−389.
(58) Li, S.; Ali, S.; Zuhra, Z.; Abbas, Y.; Xie, G.; Wang, X.; Ding, S. Turning Precious Metal-Loaded e-Waste to Useful Catalysts: Investigation into Supercilious Recovery and Catalyst Viability for Peroxymonosulfate Activation. *Chemosphere* **2023**, *336*, No. 139170.
(59) Pang, S. K.; Yung, K. C. Prerequisites for Achieving Gold Adsorption by Multiwalled Carbon Nanotubes in Gold Recovery. *Chem. Eng. Sci.* **2014**, *107*, 58−65.
(60) Sedeño-Díaz, J. E.; López-López, E.; Mendoza-Martínez, E.; Rodríguez-Romero, A. J.; Morales-García, S. S. Distribution Coefficient and Metal Pollution Index in Water and Sediments: Proposal of a New Index for Ecological Risk Assessment of Metals. *Water* **2020**, *12* (1), 29.
(61) Rahbari, M.; Goharrizi, A. S. Adsorption of Lead(II) from Water by Carbon Nanotubes: Equilibrium, Kinetics, and Thermodynamics. *Water Environment Research* **2009**, *81* (6), 598−607.
(62) Forghani, M.; Azizi, A.; Livani, M. J.; Kafshgari, L. A. Adsorption of Lead(II) and Chromium(VI) from Aqueous Environment onto Metal-Organic Framework MIL-100(Fe): Synthesis, Kinetics, Equilibrium and Thermodynamics. *J. Solid State Chem.* **2020**, *291*, No. 121636.
(63) OriginLab Corporation, Northampton, MA, USA.
(64) Belhachemi, M.; Addoun, F. Comparative Adsorption Isotherms and Modeling of Methylene Blue onto Activated Carbons. *Appl. Water Sci.* **2011**, *1* (3−4), 111−117.

https://doi.org/10.1021/acs.inorgchem.4c03407
Inorg. Chem. 2024, 63, 18992−19001